Catalysis Today 281 (2017) 21–28

Contents lists available at ScienceDirect

Catalysis Today

journal homepage: www.elsevier.com/locate/cattod

# The fabrication of $TiO_2$ supported on slag-made calcium silicate as low-cost photocatalyst with high adsorption ability for the degradation of dye pollutants in water

Jiayuan Shi[a,b], Yasutaka Kuwahara[a,c], Taicheng An[b,**], Hiromi Yamashita[a,c,*]

[a] Division of Materials and Manufacturing Science, Graduate School of Engineering, Osaka University, Osaka, Japan
[b] State Key Laboratory of Organic Geochemistry and Guangdong Key Laboratory of Environmental Protection and Resources Utilization, Guangzhou Institute of Geochemistry, Chinese Academy of Sciences, Guangzhou 510640, China
[c] Unit of Elements Strategy Initiative for Catalysts & Batteries (ESICB), Kyoto University, Katsura, Kyoto, Japan

ARTICLE INFO

*Article history:*
Received 8 January 2016
Received in revised form 19 March 2016
Accepted 21 March 2016
Available online 14 April 2016

*Keywords:*
Blast furnace slag
Calcium silicate
Titania
Photocatalysis

ABSTRACT

In this work, a composite photocatalyst of $TiO_2$ supported on the slag-made calcium silicate ($TiO_2$/SCS) was synthesized by employing a facile mixing process and using blast furnace slag as a low-cost and abundant precursor of SCS. The characterization results revealed that the open framework structure of SCS was covered by well-dispersed $TiO_2$ nanoparticle aggregates, indicating the close combination of titania and calcium silicate in the $TiO_2$/SCS photocatalyst. Higher specific surface areas could be obtained for $TiO_2$/PCS (PCS: pure calcium silicate) and $TiO_2$/SCS composites, indicating their better adsorption capabilities than that of bare $TiO_2$. The degradation of methylene blue (MB) by $TiO_2$, $TiO_2$/PCS and $TiO_2$/SCS composites with different weight percentages of titania was carried out under UV-light irradiation to systematically investigate their photocatalytic activities, and the $TiO_2$ content of 60 wt% ($TiO_2$-60/SCS) was found to be the best one to achieve the maximum rate of MB degradation, which may be due to the high specific surface area and good adsorption capacity of the composite photocatalysts. The degradation of methyl violet (MV) and methyl orange (MO) dyes indicated that the obtained photocatalysts can effectively adsorb cationic molecules (MB and MV) but have little absorption toward negatively charged molecules (MO), which play a key role in the subsequent photocatalytic degradation of dye pollutants.


## 1. Introduction

Blast furnace slag (BFS) is a major by-product generated from iron making industry. The annual discharge amounts of BFS are more than 24 million tons in Japan, over 100 million tons in China and 200 million tons in the world [1]. Its accumulation will not only occupy land, but also pollute the surrounding soil and water. Consequently, the recovery and utilization of BFS is an urgent issue worldwide. Currently, BFS is usually recycled as raw materials to produce concrete and cement [2]. However, the commercial value of these products is not so high. BFS contains a great amount of CaO, $SiO_2$, $Al_2O_3$, MgO and also incorporates other kinds of metallic elements such as Fe, Ti and Mn [3]. Fully developing and utilizing these natural components in BFS is still an important task for the sustainable development of metallurgical industry. Recently, Gong et al. fabricated BFS/$Ca(OH)_2$ sorbents in the presence of hydrated lime and used it for flue gas desulfurization [4,5]. Yamasaki et al. reported the synthesis of monolithic tobermorite from BFS for removal of heavy metal ions in water [6].

Our team reported several novel recycling processes for BFS. For example, hydroxyapatite and zeolite composite could be obtained from BFS by treating with $H_3PO_4$ and NaOH successively. The adsorption experiments indicated their great adsorption performance toward volatile organic compounds, fatty acid and proteins [7,8]. A Ca-based layered double hydroxide compound was also synthesized from the leaching solution of acid-treated BFS, and the obtained layered compound can act as a solid base catalyst in several industrially important reactions [9,10]. Apart from these, slag-made calcium silicate hydrate (SCS) was fabricated *via* a dissolution-coprecipitation method using HCl and NaOH, respectively, and the synthesized SCS was found to show good adsorption property for the removal of $Cu^{2+}$ and proteins diluted in water, demonstrating this material a promising adsorbent for water purification [11]. The above conversion processes enable us to fabricate various valuable functional materials from BFS. The catalysts and

* Corresponding author at: Division of Materials and Manufacturing Science, Graduate School of Engineering, Osaka University, Osaka, Japan.
** Corresponding author.
*E-mail addresses:* antc99@gig.ac.cn (T. An), yamashita@mat.eng.osaka-u.ac.jp (H. Yamashita).

http://dx.doi.org/10.1016/j.cattod.2016.03.039
0920-5861/

adsorbents obtained from BFS can be used for $CO_2$ fixation and water purification, thus decreasing the cost of material fabrication for the environmental remediation.

The combination of adsorbents and photocatalysts such as $TiO_2$ nanoparticles has attracted much attention for the enhanced catalytic performance of photocatalysts [12,13]. For example, it is reported that nano-structured calcium silicate-$TiO_2$ composite materials exhibited high photocatalytic degradation efficiency of phenolphthalein [14]. However, the analytical reagents containing $Ca^{2+}$ or $H_3SiO_4^-$ ions used in the preparation of pure calcium silicate (PCS) are expensive for large-scale production, and the productive effect that calcium silicate offers on the catalytic activity has not been fully investigated. The diversification of BFS treatment implemented by the above conversion methods is helpful to solve waste management problems and decrease the environment stress caused by industrial development.

Thus, in the present study, a composite photocatalyst of $TiO_2$ supported on the slag-made calcium silicate ($TiO_2$/SCS) was newly synthesized using blast furnace slag as a low-cost and abundant precursor of SCS, and the structural characterization of the obtained composite photocatalysts was investigated by XRD, SEM, FT-IR and $N_2$ adsorption. To evaluate their adsorption and photocatalytic property, three kinds of dye solutions were employed in the photocatalytic degradation experiments by using $TiO_2$/SCS composite photocatalysts with different $TiO_2$ mass contents, which were compared with $TiO_2$/PCS composite analogues and pure $TiO_2$ photocatalyst.

## 2. Experimental

### 2.1. Materials

The BFS material was provided by Nippon Steel & Sumitomo Metal Corp. The chemical composition of BFS used in this study was CaO: 40.09, $SiO_2$: 34.58, $Al_2O_3$: 14.78, MgO: 5.29, $Fe_2O_3$: 1.53, $TiO_2$: 0.78, MnO: 0.27 (wt%). Prior to the synthesis, the BFS was ball milled at 650 rpm and screened using a 45-μm mesh to facilitate dissolution. Titania nanoparticles called ST-01 were purchased from Ishihara Sangyo Kaisha, Ltd., Japan. All the other reagents such as sodium metasilicate ($Na_2SiO_3{\cdot}9H_2O$, >99%), calcium chloride ($CaCl_2$), hydrochloric acid (HCl) and sodium hydroxide (NaOH) of analytical grade were received from Wako Pure Chemical Ind. Ltd., Japan.

### 2.2. Synthesis of $TiO_2$/SCS and $TiO_2$/PCS photocatalysts

The synthesis of SCS and PCS was carried out according to the method reported previously [11]. For SCS preparation, 10.0 g of the ball-milled slag was dispersed into 200 mL of 3 M HCl aqueous solution with continuous stirring for 2 h. Then pH of the solution was adjusted to 11.0 ± 0.1 with a dropwise addition of 2 M NaOH aqueous solution. After stirring for 1 h at 100 °C, the reaction solution was aged in a Teflon container at the same temperature for another 18 h. Then the obtained product was collected by filtration, washed with a large amount of deionized water and dried at 100 °C overnight to yield SCS as a pale brown-colored powder. For PCS preparation, 0.1 mol of $Na_2SiO_3{\cdot}9H_2O$ and an equivalent mole of $CaCl_2$ were mixed in water. After adjusting the pH to 11.0 ± 0.1, the reaction solution was stirred at 100 °C for 2 h and then aged in a Teflon container at the same temperature for another 18 h. The PCS powder was obtained after filtering, washing with a copious amount of deionized water and drying at 100 °C overnight.

For $TiO_2$/SCS preparation, the desired amount of SCS was mixed with a certain amount of ST-01 ($TiO_2$) in 20 mL of isopropanol with ultrasonic dispersing for 30 min and stirring for 2 h. The solvent was removed by rotary evaporation. Finally, the products were dried under vacuum and calcined at 400 °C for 6 h to give $TiO_2$/SCS with different $TiO_2$ mass contents (*i.e.* $TiO_2$-*X*/SCS, where *X* represents the $TiO_2$ mass ratio, as shown in Table 1). $TiO_2$/PCS was also prepared with a similar procedure except that PCS was used instead of SCS.

### 2.3. Catalyst characterization

Powder X-ray diffraction (XRD) patterns were recorded using a Rigaku Ultima (IV) diffractometer with CuKa radiation (λ = 1.54056 Å). Scans were performed at step size 0.02° over 2θ range of 10–70°. The morphology of the particles was observed by field emission scanning electron microscopy (FE-SEM) in a HITACHI S-4800 field emission scanning electron microscope. Infrared spectra were recorded with a JASCO FTIR-6700 instrument in the spectral range 2000–400 $cm^{-1}$ under vacuum with a resolution of 4 $cm^{-1}$ using samples diluted with KBr. The $N_2$ adsorption measurements were performed by using a BELSORP-max system (MicrotracBEL Corp.) at −196 °C. The specific surface area was calculated by the BET (Brunauer–Emmett–Teller) method using adsorption data ranging from $P/P_0$ = 0.05 to 0.25. The pore size distributions were obtained from the adsorption branch of the nitrogen isotherms by the BJH (Barret–Joyner–Halenda) method. The ζ-potential analysis was conducted on samples dispersed in distilled water using a Zetasizer nano ZS (Malvern).

### 2.4. Photocatalytic activity test

Photocatalytic degradation of methylene blue (MB) in water was performed at room temperature under UV-light irradiation to investigate the catalytic performance of photocatalysts. The corresponding apparatus for photocatalytic degradation is shown in

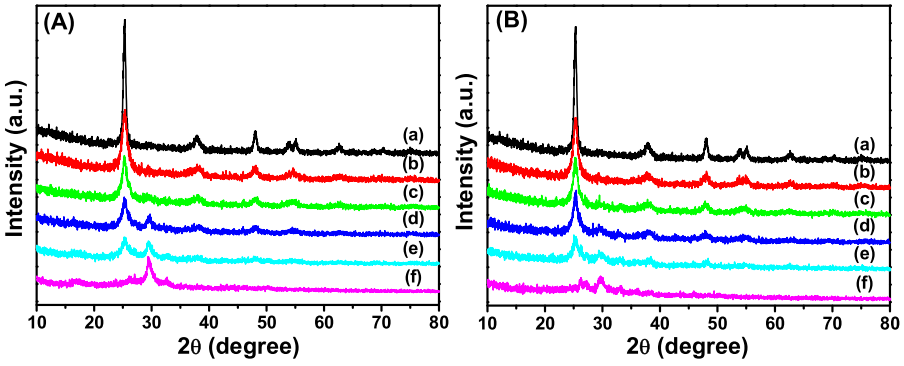


**Fig 1.** XRD patterns of (A) $TiO_2$-X/PCS samples ((a) $TiO_2$, (b) $TiO_2$-80/PCS, (c) $TiO_2$-60/PCS, (d) $TiO_2$-40/PCS, (e) $TiO_2$-20/PCS, (f) PCS) and (B) $TiO_2$-X/SCS samples ((a) $TiO_2$, (b) $TiO_2$-80/SCS, (c) $TiO_2$-60/SCS, (d) $TiO_2$-40/SCS, (e) $TiO_2$-20/SCS, (f) SCS) after sintering at the temperature of 400 °C.

**Table 1**
Composition and structural property of the composites.

| Sample | $TiO_2$ content (wt%) | BET surface area[a] ($m^2/g$) | Total pore volume[b] ($cm^3/g$) | Average pore size[c] (nm) |
|---|---|---|---|---|
| SCS | 0 | 239 | 0.81 | 1.34 |
| $TiO_2$-20/SCS | 20 | 202 | 0.54 | 2.03 |
| $TiO_2$-40/SCS | 40 | 154 | 0.59 | 2.08 |
| $TiO_2$-60/SCS | 60 | 149 | 0.57 | 2.03 |
| $TiO_2$-80/SCS | 80 | 114 | 0.57 | 1.34 |
| $TiO_2$ | 100 | 96 | 0.59 | 35.2 |
| PCS | 0 | 193 | 0.61 | 2.03 |
| $TiO_2$-20/PCS | 20 | 175 | 0.62 | 2.08 |
| $TiO_2$-40/PCS | 40 | 140 | 0.50 | 1.34 |
| $TiO_2$-60/PCS | 60 | 126 | 0.52 | 1.34 |
| $TiO_2$-80/PCS | 80 | 112 | 0.50 | 1.34 |

[a] Determined by BET methord.
[b] Defined at $P/P_0 = 0.99$.
[c] Determined from BJH pore size distribution curve.

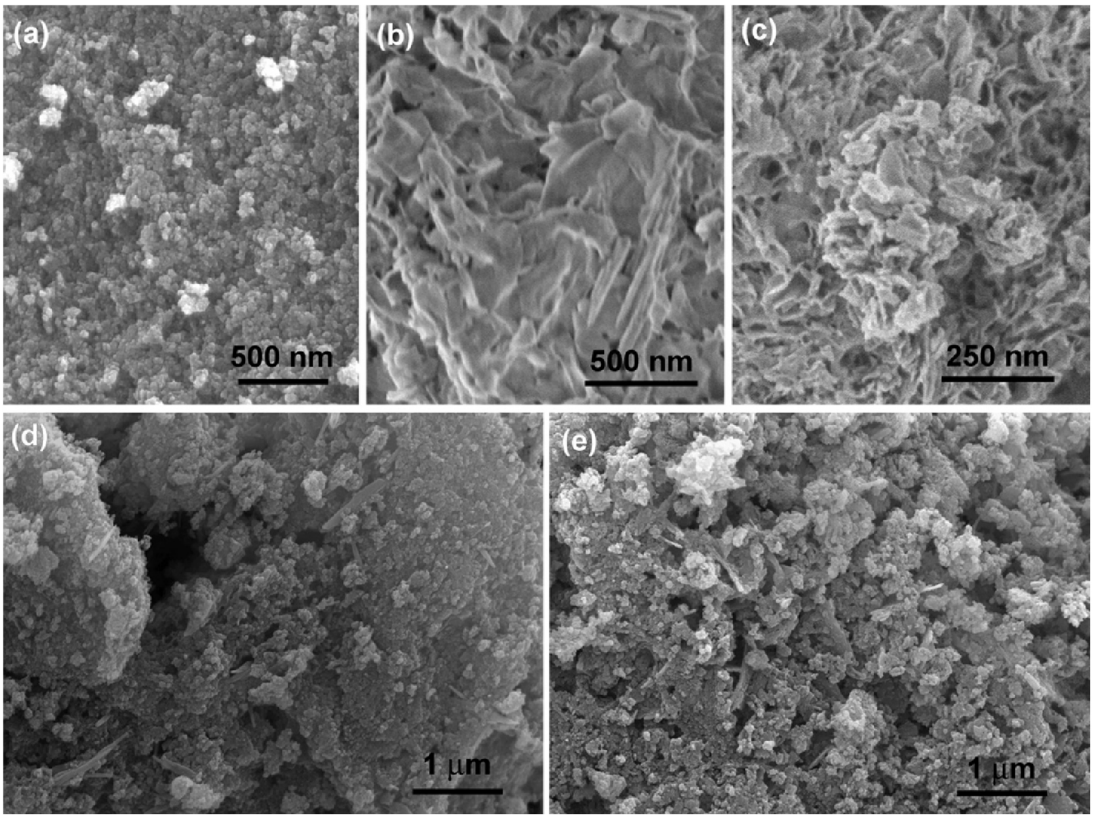


**Fig. 2.** FE-SEM images of (a) titania particles, (b) PCS, (c) SCS, (d) $TiO_2$-60/PCS and (e) $TiO_2$-60/SCS.

Fig. S1. A 100 W high-pressure Hg lamp was used as the light source (intensity = 4500 $\mu W/cm^3$, $\lambda$ = 360 nm). For all the degradation experiments in the presence of catalysts, the adding amount of catalyst was adjusted to be the same (20 mg) to fairly compare both adsorption and photocatalytic degradation percentages. In a typical test, 20 mg of photocatalyst was dispersed into 40 mL of MB solution (0.2 mM). The mixture was stirred in the dark for 60 min to allow adsorption of MB. The light source was set about 10 cm away from the liquid surface of the suspension. Then the mixture was irradiated under UV lamp to initiate the photocatalytic degradation of MB. During the reaction, at given time intervals (1 h), 2 mL of suspension was collected, filtered and 10-fold diluted with pure water, and then analyzed by a Shimadzu UV-2450 UV–vis spectrophotometer by reading the adsorption intensity at 664 nm for MB. Evolution of $CO_2$ was analyzed with a gas chromatograph equipped with a Porapack Q column, which was connected to a thermal conductivity detector (TCD).

The removal percentage ($\eta$) of MB can be calculated as follows:

$$\eta(\%) = (C_o - C_t)/C_o \times 100 \quad (1)$$

where $C_o$ and $C_t$ are the MB concentrations at initial time and after reaction period of t (h) under UV-light irradiation, respectively.

The similar experiments were carried out for 0.2 mM of methylene violet (MV, at 590 nm) and methyl orange (MO, at 464 nm) dyes to investigate the degradation activity under UV-light irradiation. To examine the catalyst reusability, the reaction suspension after the photocatalytic test was exposed under UV-light irradiation for a longer time, and the used catalyst was collected through centrifugation, washed by using ethanol for several times to ensure the removal of organic content and then subjected to next catalytic runs.

## 3. Results and discussion

### 3.1. Catalyst characterization

To characterize the crystalline structure of the samples, the XRD patterns of pure $TiO_2$, PCS and $TiO_2$-X/PCS with different $TiO_2$ contents (20%, 40%, 60% and 80%) were obtained as shown in Fig. 1a. For pure $TiO_2$, the diffraction peaks at 25.1, 37.8, 47.9, 53.9, 55.3, 62.6, 68.8, 70.2 and 75.2° correspond to (101), (004), (200), (105), (211), (204), (116), (220) and (215) planes of anatase (JCPDS card no. 89-4921), respectively, which suggests the sintered $TiO_2$ particles was solely anatase phase [15,16]. For PCS, the diffraction peaks at 17.5, 29.6, 34.3 and 50.1° correspond to (011), (112), ($\bar{1}$12) and (332) planes of calcium silicate (JCPDS card no. 89-6267), respectively [11]. The characteristic peaks of calcium silicate were found in the XRD pattern of SCS, including peaks at 17.1, 29.7 and 34.1°. However, the diffraction peaks of SCS at 26.2 or 27.3° do not clearly appear in the pattern of PCS. They can be attributed to calcium aluminum silicate, indicating the compositional difference between PCS and SCS [17]. The XRD patterns of $TiO_2$-X/PCS have two characteristic peaks at 25.4° and 29.7° corresponding to the (101) crystal facet of anatase phase and (112) crystal facet of calcium silicate, respectively [18,19]. The peak intensities of anatase phase become stronger as the mass ratio of $TiO_2$ in photocatalysts increases, while the opposite tendency is obtained for the diffraction peaks of calcium silicate. Similar results can be obtained for those of $TiO_2$-X/SCS (Fig. 1b).

The FE-SEM technique was used to investigate the morphology and microstructure of $TiO_2$-60/PCS and $TiO_2$-60/SCS powders, as shown in Fig. 2. For comparison, pure titania particles, PCS and SCS were also observed. The calcined titania sample in Fig. 2a is consisted of roundish nanoparticles with the size of 30–50 nm. The PCS in Fig. 2b shows bulk structures with the diameter of several hundred nanometers. The SCS in Fig. 2c shows aggregated flacks with the size exceeding 100 nm. These flack aggregates have an open framework structure, indicating that SCS has a large surface area which might be useful for the adsorption of organic pollutants. The particle diameters of PCS and SCS are significantly larger than those of $TiO_2$ nanoparticles. For $TiO_2$-60/PCS and $TiO_2$-60/SCS, their surfaces are much coarser than those of PCS and SCS, indicating that PCS and SCS are covered by well-dispersed $TiO_2$ nanoparticle aggregates (Fig. 2d and Fig. 2e). It is assumed that $TiO_2$ small nanoparticles are physically adsorbed onto the PCS and SCS *via* the Van der Waals forces among particles and the interaction between Ti-OH and Mi-OH (M = Ca, Si and Al *etc.*) species on the support surfaces [20–23].

A detailed analysis of the structure of photocatalysts was performed by infrared spectroscopy. Fig. 3 shows the FT-IR spectra of pure $TiO_2$, PCS, SCS, $TiO_2$-60/PCS and $TiO_2$-60/SCS. All of the spectra show a weak peak at around 1644 $cm^{-1}$ and a strong peak near 462 $cm^{-1}$, which can be attributed to the O—H bending vibration of hydroxyls or molecular $H_2O$ and the deformation of $TO_4$ tetrahedra (T = Ti, Si, Al, Mg, *etc.*) [24,25]. In the spectra of PCS, SCS, $TiO_2$-60/PCS and $TiO_2$-60/SCS, the absorption peak at 857 $cm^{-1}$ and 1492 $cm^{-1}$ can be attributed to carbonate species ($CO_3^{2-}$) adsorbed on the Ca sites [26]. The intense band present near 1000 $cm^{-1}$ belongs to the asymmetric stretching mode of Si—O or Si—O—Si groups. In comparison with the peak of Si—O stretching modes at 1025 $cm^{-1}$ for the pure silica in previous report [27], the corresponding peaks of PCS and SCS in Fig. 3 red-shift to 983 and 994 $cm^{-1}$ respectively, owing to the formation of Si—O—Ca bonding [11]. The corresponding peaks are also shown in $TiO_2$-60/PCS and $TiO_2$-60/SCS at similar positions (990 and 1001 $cm^{-1}$, respectively), indicating that the Si—O—Ca networks in the calcium silicates have been preserved even after the $TiO_2$ deposition [28,29].

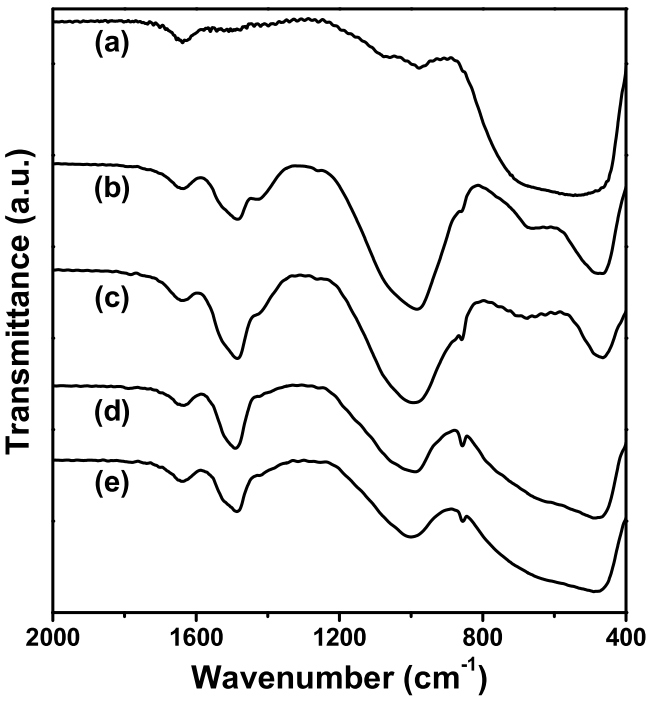


**Fig. 3.** FTIR spectra of (a) pure $TiO_2$, (b) PCS, (c) SCS, (d) $TiO_2$-60/PCS and (e) $TiO_2$-60/SCS.

The porous structure and BET surface areas of the photocatalysts were also investigated by nitrogen adsorption–desorption. Fig. 4 displays the nitrogen sorption isotherms for the pure $TiO_2$, PCS, SCS, $TiO_2$-X/PCS and $TiO_2$-X/SCS samples. The nitrogen sorption isotherms for all of the photocatalysts are similar and display hysteresis loops at higher relative pressure region ($P/P_0 > 0.8$), indicating the presence of intra- and inter-crystalline mesoporosity, which can be categorized as type IV according to IUPAC classification [30,31]. The isotherms of PCS, SCS, $TiO_2$-X/PCS and $TiO_2$-X/SCS exhibit H3 hysteresis loops associated with the presence of slit-like pores. However, the isotherm of pure $TiO_2$ exhibits H1 hysteresis loop which is the typical feature of cylinder-type mesopores [30,31]. Table 1 show that all the $TiO_2$-X/SCS and $TiO_2$-X/PCS samples have larger specific surface areas than pure $TiO_2$. This is because the combination with calcium silicates (SCS or PCS) has higher surface area than that of $TiO_2$. It is reasonable to conclude that the BET specific surface area increases with increasing the amount of calcium silicate. The specific surface areas of SCS and $TiO_2$-X/SCS are higher than those of PCS as well as the corresponding $TiO_2$-X/PCS, respectively, indicating the slag-derived impurity elements have an ability to increase the porosity of calcium silicate [11]. In addition, the pore diameter and pore volumes derived from the nitrogen adsorption/desorption isotherms of the samples are also listed in Table 1. The pore volume of all the samples ranges from 0.5 to 0.81 $cm^3/g$, while the pore size centers at 1–3 nm except for the pure $TiO_2$.

### 3.2. Photocatalytic degradation of MB by $TiO_2$-X/SCS

The photocatalytic degradation of MB was performed under UV-light irradiation by using $TiO_2$-X/SCS as photocatalysts to examine their photocatalytic activities. For comparison, SCS, PCS and pure $TiO_2$ were also tested. Fig. 5 shows the results of MB decomposition under UV-light irradiation in the presence of SCS, pure $TiO_2$ and $TiO_2$-X/SCS photocatalysts. Before the photocatalysis, the adsorption performance of photocatalysts was investigated, because the adsorption serves as a key process in removing the

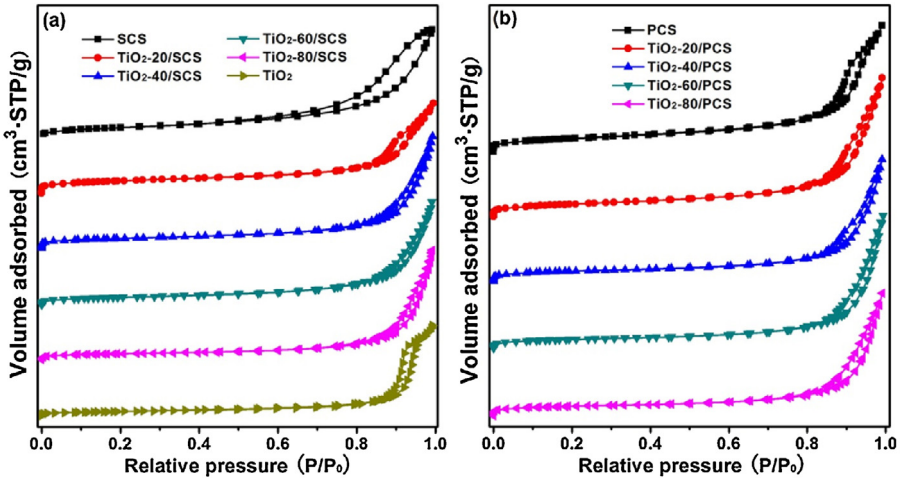


**Fig. 4.** Nitrogen adsorption–desorption isotherms of (a) SCS, $TiO_2$-X/SCS and pure $TiO_2$; (b) PCS and $TiO_2$-X/PCS.

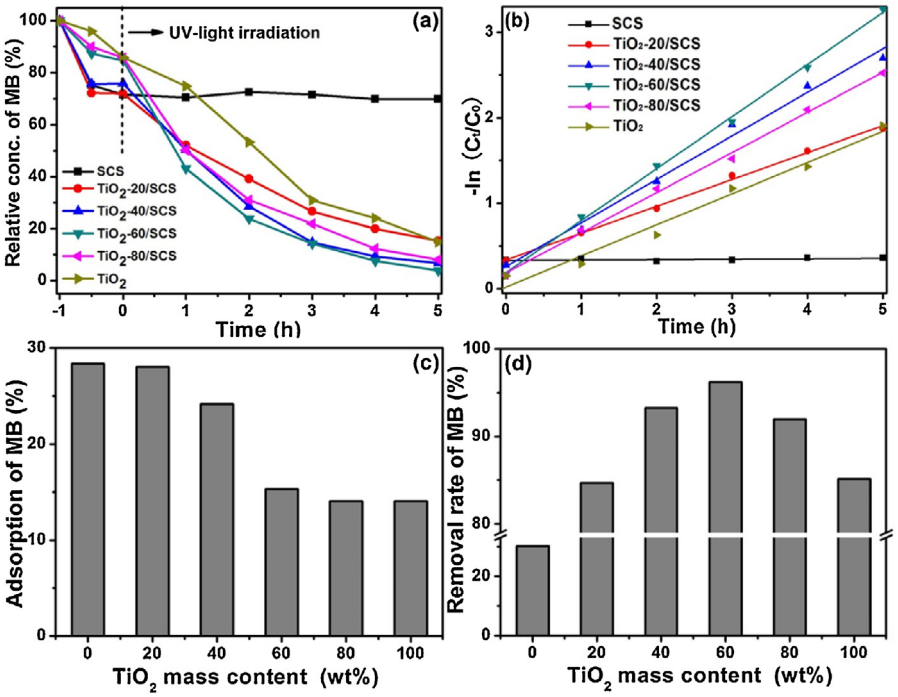


**Fig. 5.** (a) Degradation profile and (b) kinetic parameters of methylene blue (MB) degradation under UV-light irradiation in the presence of SCS, pure $TiO_2$ and $TiO_2$/SCS with different $TiO_2$ mass contents; The dependence of (c) adsorption and (d) removal rate of MB on $TiO_2$ mass content.

dissolved organic pollutants. As shown in Fig. 5c, the adsorption property of SCS (28.4%) is much better than that of pure $TiO_2$ (14.0%). As expected, the results in Fig. 5a and c demonstrate that the adsorption efficiencies of MB decrease with the increase of $TiO_2$ mass contents in $TiO_2$-X/SCS, following the order of $TiO_2$-20/SCS (28.0%) > $TiO_2$-40/SCS (24.2%) > $TiO_2$-60/SCS (15.3%) > $TiO_2$-80/SCS (14.2%). It is probably due to the large surface area of SCS and its effective adsorption of organic cations such as positively charged MB molecule [32]. To investigate the adsorption behavior between $TiO_2$-X/SCS and MB molecules, the ζ-potential measurements of $TiO_2$-60/SCS is also carried out to provide a quantitative analysis of the surface charge. As a result, the negative-charged nature of the $TiO_2$-60/SCS surface (−17.5 mV) is confirmed. This implies that the cationic MB molecules can be adsorbed easily onto the $TiO_2$-X/SCS surface. Specifically, the weakly bonded $Ca^{2+}$ and other metal ions in SCS are released into the solution, leaving electronegative silicate network in SCS. As a result, the material surface becomes negatively charged and attracts cationic molecules [11]. In addition, the large surface area of SCS helps to increase the dispersion of $TiO_2$ nanoparticles onto the SCS support, which can efficiently reduce the particle aggregation and enhance the photon absorption of $TiO_2$ [33–35]. Under UV light irradiation, the removal of MB in Fig. 5d follows the order of $TiO_2$-60/SCS (96.2%) > $TiO_2$-40/SCS (93.2%) > $TiO_2$-80/SCS (92.0%) > $TiO_2$ (85.1%) > $TiO_2$-20/SCS (84.7%) > SCS (30.1%), which is different from the order of the adsorption. The adsorption and removal rate of $TiO_2$-60/SCS are 1.3% and 11.1% higher than those of pure $TiO_2$, respectively. For all the photocatalysts, the photocatalytic degradation of MB follows a pseudo first order rate law. The highest activity is achieved for $TiO_2$-60/SCS with a rate constant of 0.61 $h^{-1}$, and the lowest rate constant of 0.31 $h^{-1}$ is obtained for

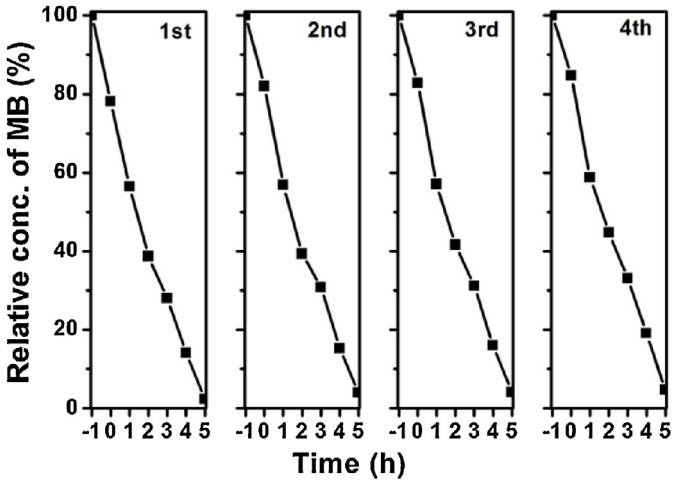


**Fig. 6.** Photocatalytic performance of $TiO_2$-60/SCS in 4 cyclic degradation tests.

$TiO_2$-20/SCS (Fig. 5b). The degradation of MB was hardly observed in the absence of photocatalysts under UV-light irradiation. The removal of MB in the presence of $TiO_2$-60/SCS or $TiO_2$-60/PCS without light irradiation was also very limited (Fig. S2). It indicates that the observed dye removal can be mainly attributed to the light-induced photocatalytic degradation by $TiO_2$. Fig. S3 shows the amount of $CO_2$ evolved during the degradation of MB. The amount of $CO_2$ increased gradually with increasing UV-light irradiation time, indicating that the organic molecules were ultimately mineralized into $CO_2$ and water. In the presence of $TiO_2$-60/SCS or $TiO_2$-60/PCS, the $CO_2$ yield in the dark can be negligible, and only a little $CO_2$ was produced in the absence of catalysts under UV-light irradiation, proving that the formation of $CO_2$ is mainly due to the photocatalytic degradation of MB. The $CO_2$ yield during the photocatalytic degradation of MB under UV-light irradiation follows the order of $TiO_2$-60/SCS > $TiO_2$-60/PCS > $TiO_2$, indicating the improved photocatalytic activity of $TiO_2$-60/SCS and $TiO_2$-60/PCS composites compared with that of unsupported $TiO_2$. The concentration of MB in the presence of SCS shows very little change after 5 h UV-light irradiation, indicating a negligible photocatalytic activity of SCS (Fig. 5a). For all the experiments of photocatalytic degradation, the addition amount of photocatalyst is unchanged (20 mg). Therefore, when the SCS content increases from 0% (0 mg) to 80% (16 mg), the $TiO_2$ amount in the photocatalyst will decrease from 100% (20 mg) to 20% (4 mg). In other words, the introduction of SCS into the prepared photocatalysts can improve the adsorption capability but weaken the photocatalytic activity of materials. As a result, the degradation activity of photocatalysts appears a maximum of 96.2% when the mass ratio of $TiO_2$ is 60%. Furthermore, four-recycle experiments demonstrate that $TiO_2$-60/SCS maintains a high degradation efficiency of *ca.* 95% after four continuous recycles, suggesting the high photocatalytic stability of the synthesized composite photocatalysts (Fig. 6).

### 3.3. Photocatalytic degradation of MB by $TiO_2$-X/PCS

The photocatalytic activity of $TiO_2$-X/PCS was also investigated through MB degradation under UV-light irradiation. The degradation curves, kinetic parameters, adsorption and degradation efficiency are also summarized in Fig. 7a–d. The photocatalytic degradation rate of PCS is close to zero indicating a negligible photocatalytic activity of PCS. The adsorption capabilities of $TiO_2$-X/PCS with different $TiO_2$ mass ratios remain constant (Fig. 7c), probably because PCS (14.8%) has the equivalent adsorption performance to that of pure $TiO_2$ (14.0%). Compared with the photocatalytic activity of pure $TiO_2$ (85.1%), there is no obvious activity improvement for $TiO_2$-40/PCS (85.9%), $TiO_2$-60/PCS (87.8%) and $TiO_2$-80/PCS (84.0%) after combining PCS with $TiO_2$ photocatalysts (Fig. 7d). Moreover, the rate constants of photocatalytic degradation of $TiO_2$-40/PCS (0.35 $h^{-1}$), $TiO_2$-60/PCS (0.37 $h^{-1}$), $TiO_2$-80/PCS (0.34 $h^{-1}$) and pure $TiO_2$ (0.36 $h^{-1}$) are also similar (Fig. 7b).

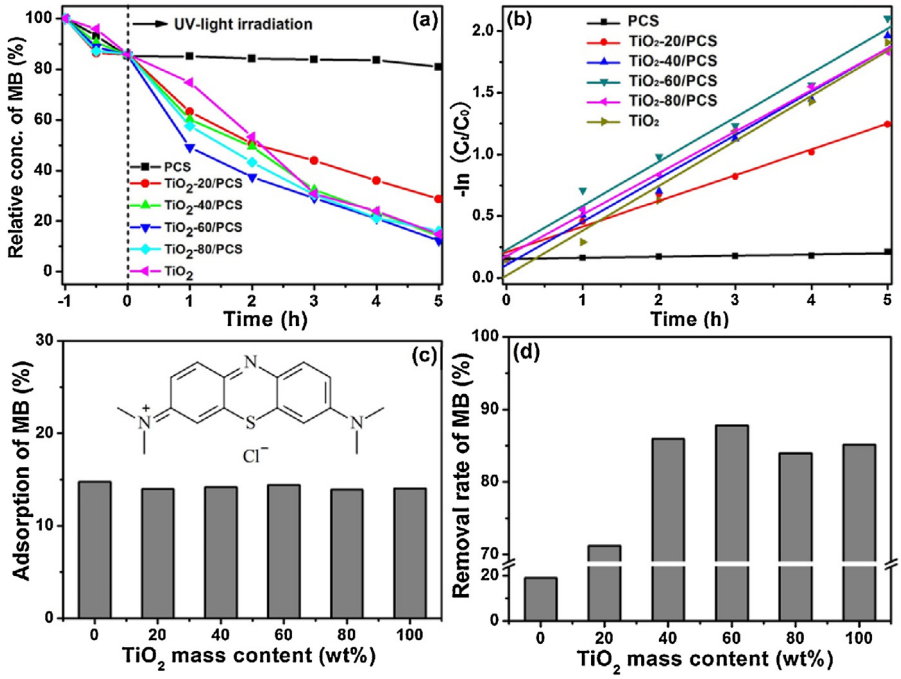


**Fig. 7.** (a) Degradation profile and (b) kinetic parameters of MB degradation under UV-light irradiation in the presence of PCS, pure $TiO_2$ and $TiO_2$/PCS with different $TiO_2$ mass contents; The dependence of (c) adsorption and (d) removal rate of MB on $TiO_2$ mass content. Inset of (c): molecular structure of MB.

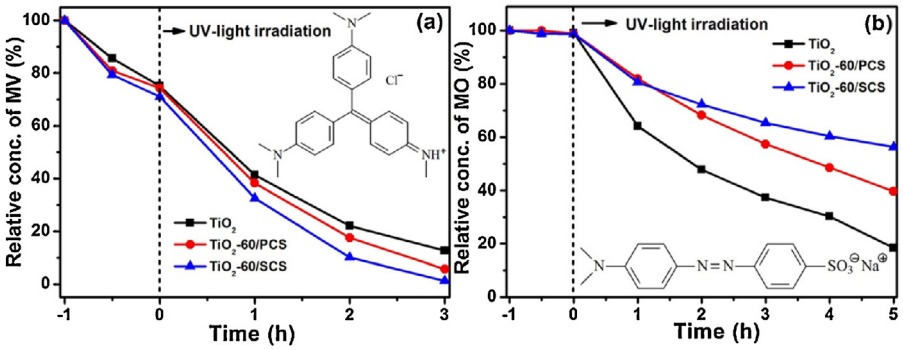


**Fig. 8.** Photocatalytic degradation of (a) methyl violet (MV) and (b) methyl orange (MO) under UV-light irradiation in the presence of $TiO_2$, $TiO_2$-60/PCS and $TiO_2$-60/SCS. Insets of (a) and (b): molecular structures of MV and MO.

### *3.4. Comparison of the photocatalytic degradation of MV and MO by $TiO_2$-X/PCS and $TiO_2$-X/SCS*

The photocatalytic activities of $TiO_2$-60/SCS, $TiO_2$-60/SCS and pure $TiO_2$ in the degradation of MV and MO dyes were also investigated (Fig. 8). The initial concentration of dyes remains the same (0.2 mM) under all experimental condition. While dissolving in the aqueous solution, MV and MO dyes are positively and negatively charged, respectively (Insets of Fig. 8a and b). In the case of MV degradation, $TiO_2$-60/SCS (28.9%) shows a higher adsorption capacity and photocatalytic activity is a little higher than those of pure $TiO_2$ (24.9%, Fig. 8a), which is similar to the case of MB degradation. It is mainly due to the effective adsorption of organic cations such as MB (inset of Fig. 7c) and MV molecules in the presence of SCS adsorbent. Moreover, both adsorption amount and degradation rate of $TiO_2$-60/SCS (28.9%, 1.34 $h^{-1}$) are higher than those of $TiO_2$-60/PCS (25.4%, 0.85 $h^{-1}$), respectively. This may be due to the limited adsorption capability of PCS, which has less influence on the photocatalysis compared with that of $TiO_2$-60/SCS photocatalyst. Compared with $TiO_2$-60/PCS, $TiO_2$-60/SCS can provide a higher adsorption capability and an improved photocatalytic activity. The improved adsorption performance of $TiO_2$-60/SCS can be elucidated from the following two results: (i) the higher specific surface area of SCS (239 $m^2$/g) than that of PCS (193 $m^2$/g, Table 1); (ii) the more negative ζ-potential of SCS (−17.5 mV) than that of PCS (−15.7 mV). These results indicate that SCS can be used as an effective support material for $TiO_2$ photocatalysts.

In the case of MO degradation, however, pure $TiO_2$ (0.96%), $TiO_2$-60/PCS (1.16%) and $TiO_2$-60/SCS (1.35%) show almost no adsorption of MO, indicating that neither $TiO_2$ nor calcium silicate (PCS or SCS) can adsorb negatively charged organic molecules. As a result, $TiO_2$-60/PCS (60.3%) and $TiO_2$-60/SCS (43.7%) show low photocatalytic activities, while pure $TiO_2$ (81.5%) has the best performance for MO degradation. The photocatalytic degradation rates constant decrease in the order of $TiO_2$ (0.31 $h^{-1}$) > $TiO_2$-60/PCS (0.18 $h^{-1}$) > $TiO_2$-60/SCS (0.11 $h^{-1}$). These results indicate the important role of adsorption in the photocatalytic degradation. The adsorption step determines the speed of mass transportation in the photocatalytic process and has obvious influence on the subsequent photocatalytic degradation of organic pollutants. The interactions between photocatalysts and dyes in the solution depend not only on the specific surface area of photocatalysts, but also on the surface properties of catalysts such as ζ-potential. The negative charges of SCS (−17.5 mV) and PCS (−15.7 mV) are also confirmed through ζ-potential measurements. Therefore, both of them can act as good adsorbents for cationic dyes such as MB and MV. Compared with PCS, the increased surface negative charge of SCS is reflected in its higher adsorption ability of MB and MV. Oppositely, the electrostatic repulsion between the negatively-charged photocatalysts and anionic MO molecules hinders the adsorption of MO, which consequently results in the low degradation efficiency of MO.

## 4. Conclusions

The $TiO_2$/SCS composite photocatalysts was fabricated by a simple mixing procedure of slag-made calcium silicate (SCS) and commercial $TiO_2$ powders and was compared with the $TiO_2$ analogue supported on pure calcium silicate (PCS). The characterization results of the prepared photocatalysts showed that $TiO_2$ nanoparticles were covered onto the aggregated flack structures of SCS/PCS to form the composite photocatalysts, which indicated the close combination of $TiO_2$ and calcium silicate supports. Among the catalysts prepared, the $TiO_2$-60/SCS photocatalyst exhibited a higher photocatalytic activity than that of $TiO_2$-60/PCS in the photocatalytic degradation of cationic dyes such as MB and MV in water, which is due to the higher specific surface area and more negative ζ-potential of SCS compared with those of PCS. The comparative degradation studies using methyl violet (MV) and methyl orange (MO) dyes indicated that the obtained photocatalysts preferred the adsorption of organic cations and the subsequent degradation of cationic dye. As demonstrated in this work, BFS can be used as an economical precursor for the preparation of calcium silicate adsorbent which can replace PCS as the low-cost supporting material for $TiO_2$ photocatalysts. This study would provide a versatile and practical strategy to fabricate efficient and inexpensive photocatalysts in the application of water purification.

## Acknowledgments

This work was financially supported by China Postdoctoral Science Foundation (2014M552247), the ISIJ Research Promotion Grant (Tekkou Kenkyu Shinko Josei) awarded to Y.K. from the Iron and Steel Institute of Japan, the strategic China-Japan research cooperative program 2012 from JST and Natural Science Foundation of China (NSFC, 41425015). Y.K. thanks the financial support by a Grant-in-Aid from the Frontier Research Base for Global Young Researchers, Osaka University. The authors also acknowledge financial support from China Scholarship Council.

## Appendix A. Supplementary data

Supplementary data associated with this article can be found, in the online version, at http://dx.doi.org/10.1016/j.cattod.2016.03.039.

## References


[1] (a) W. Li, D. Weng, X. Zhang, Iron Steel Scrap China 6 (2007) 34–38;
(b) The Japan Iron and Steel Federation, Nippon Slag Association, The Annual report of statistics of Iron and Steel slag (2014) see the website, http://www.slg.jp.;
(c) U.S. Geological Survey, Iron and Steel Slag Statistics and Information, Mineral Commodity Summaries, see the website, http://minerals.usgs.gov/minerals/pubs/commodity/iron_&_steel_slag/.
[2] K. Nobata, Y. Ueki, Nippon Steel Tech. Rep. 86 (2002) 44–47.
[3] E. Douglas, R. Zerbino, Cement Concrete Res. 16 (1986) 662–670.
[4] G. Gong, S. Ye, Y. Tian, Y. Cui, Y. Chen, Ind. Eng. Chem. Res. 47 (2008) 7897–7902.
[5] G. Gong, S. Ye, Y. Tian, Q. Wang, J. Ni, Y. Chen, J. Hazard. Mater. 166 (2009) 714–719.
[6] A. Nakahira, H. Naganuma, T. Kubo, Y. Yamasaki, J. Ceram. Soc. Jpn. 116 (2008) 500–504.
[7] Y. Kuwahara, T. Ohmichi, T. Kamegawa, K. Mori, H. Yamashita, J. Mater. Chem. 19 (2009) 7263–7272.
[8] Y. Kuwahara, T. Ohmichi, T. Kamegawa, K. Mori, H. Yamashita, J. Mater. Chem. 20 (2010) 5052–5062.
[9] Y. Kuwahara, H. Yamashita, J. $CO_2$ Util. 1 (2013) 50–59.
[10] Y. Kuwahara, H. Yamashita, ISIJ Int. 55 (2015) 1531–1537.
[11] Y. Kuwahara, S. Tamagawa, T. Fujitani, H. Yamashita, J. Mater. Chem. A 1 (2013) 7199–7210.
[12] Y. Kuwahara, T. Ohmichi, K. Mori, I. Katayama, H. Yamashita, J. Mater. Sci. 43 (2008) 2407–2410.
[13] Y. Kuwahara, H. Yamashita, J. Mater. Chem. 21 (2011) 2407–2416.
[14] J.H. Johnston, A.C. Small, J. Mater. Chem. 21 (2011) 1240–1245.
[15] X. Nie, G. Li, P.-K. Wong, H. Zhao, T. An, Catal. Today 230 (2014) 67–73.
[16] P. Karthik, R. Vinoth, S.G. Babu, M. Wen, T. Kamegawa, H. Yamashita, B. Neppolian, RSC Adv. 5 (2015) 39752–39759.
[17] E. L'Hopital, B. Lothenbach, G. Le Saout, D. Kulik, K. Scrivener, Cement Concrete Res. 75 (2015) 91–103.
[18] J. Bai, Y. Li, J. Xiang, L. Ren, M. Mao, M. Zeng, X. Zhao, Chem. Asian J. 10 (2015) 1394–1401.
[19] Q. Huang, X. Liu, T.A. Elkhooly, R. Zhang, Z. Shen, Q. Feng, Colloids Surf B: Biointerfaces 134 (2015) 169–177.
[20] H.K. Mishra, M. Stanciulescu, J.P. Charland, J.F. Kelly, Appl. Surf. Sci. 254 (2008) 7098–7103.
[21] P. Li, C. Xie, J. Liu, Z. Wang, X. Xiao, Surf. Coat. Technol. 258 (2014) 624–630.
[22] N. Eom, R.B. Walsh, G. Liu, D.F. Parsons, V.S.J. Craig, Procedia Eng. 102 (2015) 24–34.
[23] S.K. Parayil, A. Razzaq, S.-I. In, J. Nanosci. Nanotechnol. 15 (2015) 7285–7292.
[24] A. Meiszterics, L. Rosta, H. Peterlik, J. Rohonczy, S. Kubuki, P. Henits, K. Sinko, J. Phys. Chem. A 114 (2010) 10403–10411.
[25] J. Matos, T. Marino, R. Molinari, H. Garcia, Appl. Catal. A: Gen. 417 (2012) 263–272.
[26] Y. Kuwahara, T. Yamanishi, T. Kamegawa, K. Mori, H. Yamashita, J. Phys. Chem. B 115 (2011) 10335–10345.
[27] J.-Y. Shi, Q.-Z. Yao, X.-M. Li, G.-T. Zhou, S.-Q. Fu, PLoS One 8 (2013).
[28] D. Scarano, A. Zecchina, S. Bordiga, F. Geobaldo, G. Spoto, G. Petrini, G. Leofanti, M. Padovan, G. Tozzola, J. Chem. Soc. Faraday Trans. 89 (1993) 4123–4130.
[29] X.T. Gao, I.E. Wachs, Catal. Today 51 (1999) 233–254.
[30] K.S.W. Sing, D.H. Everett, R.A.W. Haul, L. Moscou, R.A. Pierotti, J. Rouquerol, T. Siemieniewska, Pure Appl. Chem. 57 (1985) 603–619.
[31] P.B. Balbuena, K.E. Gubbins, Langmuir 9 (1993) 1801–1814.
[32] G. Tronci, H. Ajiro, S.J. Russell, D.J. Wood, M. Akashi, Acta Biomater. 10 (2014) 821–830.
[33] X.F. Qian, T. Kamegawa, K. Mori, H.X. Li, H. Yamashita, J. Phys. Chem. C 117 (2013) 19544–19551.
[34] W. Donphai, T. Kamegawa, M. Chareonpanich, K. Nueangnoraj, H. Nishihara, T. Kyotani, H. Yamashit, Phys. Chem. Chem. Phys. 16 (2014) 25004–25007.
[35] H.-P. Jing, C.-C. Wang, Y.-W. Zhang, P. Wang, R. Li, RSC Adv. 4 (2014) 54454–54462.